RSC Advances

ROYAL SOCIETY OF CHEMISTRY

www.rsc.org/advances

Third order NLO properties of corannulene and its Li-doped dimers: effect of the concave-convex and convex-convex stuctures

Li Wang, Wen-Yong Wang, Xin-Yan Fang, Chang-Li Zhu, Yong-Qing Qiu*

Institute of Functional Material Chemistry, Faculty of Chemistry, Northeast Normal University, Changchun, Jilin 130024, People's Republic of China

ABSTRACT

Buckybowls involving π-π interactions offer exciting future opportunities in terms of designing novel smart nonlinear optical (NLO) materials. Dimeric specie of corannulene ($C_{20}H_{10}$), the smallest buckybowl, was considered as a model for the host-guest assemblies exhibiting the convex-concave stacking of curved conjugated carbon surfaces. Different stacking motifs (concave-convex and convex-convex dimers) of $C_{20}H_{10}$ dimers in affecting the NLO properties are the focus of our work. We performed density functional theory to calculate the structure, binding interactions, electronic absorption spectra and second hyperpolarizabilities of π-stacking dimers of $C_{20}H_{10}$ and its Li-doped derivative. It is found that the concave-convex dimers exhibit the stronger binding interactions because of larger electrostatic interactions and thus are more stable with respect to the convex-convex dimers. The doping of Li ion significantly enhances the orbital interaction between the monomers but slightly effects on the spectra and the second hyperpolarizabilities of the dimers. The convex-convex dimers exhibit larger polarizabilities and second hyperpolarizabilities (γ_{zzzz}) as a result of enhanced interlayer charge transfer properties. And there is an increasing linear relationship between the electronic coupling and γ_{zzzz} values. The results presented in this article provide important evidence for the convex-convex stacking way in enhancing the NLO properties of the π-stacking dimers. Thus,

* Corresponding Author. Fax: +86 431 85098768.
E-mail addresses: qiuyq466@nenu.edu.cn (Y. Q. Qiu)

controlling molecular stacking is an important way in terms of designing novel smart NLO materials.

Keywords: Dimer; The second hyperpolarizability; Interlayer charge-transfer; DFT

1. Instruction

Buckybowls including fullerenes and carbon nanotubes have been the subject[1, 2] of intense experimental and theoretical researches in recent years because of their relation to the formation of intermolecular complexes.[3-8] In addition to having the good shape match, buckybowls have large dipole moments due to their curvatures that should provide enhanced π-π intermolecular interactions,[9-15] which are critical in determining the crystal packing.[16] The crystal packing and resulting charge transfer (CT) properties are found to be strongly connected. Because a remarkably large range of obvious CT properties can be achieved via crystal engineering of existing molecular backbones.[17] The obvious CT properties can cause a large difference between the ground and excited state dipole moments and low-energy CT transitions,[18, 19] which thus causes the organic molecules exhibiting considerably large nonlinear optical (NLO) activities.[20-24] Therefore, the π-π intermolecular interactions, connecting greatly with obvious CT properties, are found to be strongly affects the NLO properties. In view of this, buckybowls involving π-π interactions offer exciting future opportunities in terms of designing novel smart NLO materials.

The smallest buckybowl corannulene ($C_{20}H_{10}$, Scheme 1) was first prepared by Lawton and Barth in 1966.[25] Motivated by the novel bowl-shape of $C_{20}H_{10}$, studies of its surfaces have revealed a surface stereochemical principle that is optimal packing motifs of molecules in the ball- and bowl-in-bowl complexation.[26] The interesting stacking motifs are the concave-convex and convex-convex assemblies. The potential of the concave-convex stacking motif was recognized early and proposed as a major factor of gas-phase formation of dimeric species of $C_{20}H_{10}$.[27] The $C_{20}H_{10}$ dimer was considered as a model system for the host-guest assemblies exhibiting the convex-concave stacking of curved conjugated carbon surfaces.[28] Therefore, different

stacking motifs of dimeric species of $C_{20}H_{10}$ were expected to become the meaningful and novel research of adjusting the NLO properties effectively.

A lot of related studies focused on the concave-convex eclipsed $C_{20}H_{10}$ dimer.[29-34] Eclipsed and staggered dimers of $C_{20}H_{10}$ (Scheme 1) had been studied.[29] Results show that eclipsed conformations are the most stable $C_{20}H_{10}$ dimers. High level ab initio calculations on the eclipsed concave-convex corannulene dimer yielded a minimum of 15.43 kcal/mol at 3.64 Å at the counterpoise corrected QCISD(T)/aug-cc-pVTZ level. For corannulene, the eclipsed concave-convex homodimers is the global minimum.[30] In 2008,[31] theoretical calculations studied by Andrzej Sygula and Svein Saebø show that the binding energy of the native concave-convex corannulene dimer is quite substantial (17.2 kcal/mole at the best SCS-MP2/cc-pvtz level of theory) with an equilibrium distance of about 3.64 Å. In the same year, it is revealed that eclipsed concave-convex corannulene dimer yielded a binding energy of 15.5 kcal/mol with a monomer-monomer distance of 3.69 Å at the (extrapolated) counterpoise corrected QCISD(T)/aug-cc-pVTZ level.[32] In 2012, the benchmark curve shows a minimum of 15.43 kcal/mol at 3.64 Å. B3LYP-D3(BJ) exhibited smaller errors suggesting that B3LYP-D3(BJ) is optimal.[33]

Based on this result, the eclipsed and staggered configurations of the concave-convex and convex-convex corannulene dimers have been investigated. However, no final stable staggered configuration of the convex-convex corannulene dimer was obtained. The stable eclipsed configuration of the concave-convex corannulene dimer was verified by optimizing initial staggered configuration in our work. Therefore, the eclipsed stacking of $C_{20}H_{10}$ and its Li-doped dimers (Scheme 1) are investigated: the concave-convex (**1a** and **1b**) and convex-convex stacking dimers (**2a** and **2b**). Continuing our interests in the research of organic molecular materials with substantial NLO activities,[35-38] different stacking motifs (concave-convex and convex-convex dimers) in affecting interlayer CT properties and thus adjusting the NLO properties are the focus of our work. We performed density functional theory (DFT) to calculate the structures, binding interactions, electronic absorption spectra and second hyperpolarizabilities of the four dimers. Specifically, in this study, we will

mainly address the following issues: (1) predicting the stability of the concave-convex and convex-convex stacking dimers theoretically, (2) investigating Li-doped effect on the second hyperpolarizabilities of the dimers. (3) exhibiting the new structure-hyperpolarizability relationships and the dependence of the second hyperpolarizabilities on the interlayer CT property, (4) understanding the nature of the dependence of second hyperpolarizabilities on interlayer CT properties. We hope this work may evoke one's attention to design novel and highly efficient third-order NLO molecular materials with excellent building blocks (the convex-convex stacking motifs).

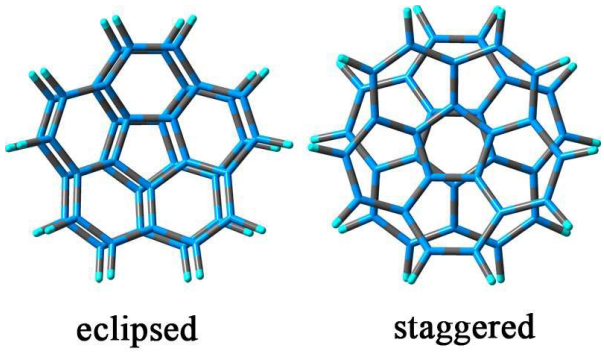

Scheme 1 Eclipsed and staggered structures of $C_{20}H_{10}$ dimers.

2. Computation details

The choice of suitable method is crucial to generate reliable and accurate results. The hybrid meta-generalized gradient-approximations M06-2X functional with the double amount of nonlocal exchange (2X) is recommended by Truhlar and Zhao.[39, 40] This functional is an excellent method for the calculation of aromatic-aromatic stacking interactions. Therefore, M06-2X was selected to optimize the geometries of the studied dimers. We have adopted the 6-31+G(d,p) basis set for C and H with exception of 6-311+G(3df) for Li ion. The large basis set 6-311+G(3df) could describe more accurately the charge transfer and dispersion effects of the metal ion. On the other hand, as for the binding energy, using large basis set 6-311+G(3df) for the Li cation gave an more accurate binding energy (34.94 kcal/mol) than 6-31+G(d,p) for the Li cation (34.55 kcal/mol). Owing to that M06-2X underestimates the binding

energies, using large basis set for the Li cation could reduce the error. Each of the geometries is locally stable with all real frequencies.

To correct the basis set superposition error (BSSE), the counterpoise (CP) procedure was used to calculate the interaction energy.[41] The interaction energy (E_{int}) can be expressed as the difference between the energy of the dimer and the sum of the energies of the monomers according to equation:

$$E_{int}(AB) = E(AB)_{AB} - [E(A)_{AB} + E(B)_{AB}] \quad (1)$$

A proper computational description of the relatively weak dispersion interactions is not trivial. Many people have used different methods to study the binding energy of concave-convex stacking dimers. The results show that the benchmark calculation of 15.5 kcal/mol was obtained at QCISD(T)/aug-cc-pVTZ level.[29] M06-2X underestimates when compared to the high level ab initio calculations at the counterpoise corrected QCISD(T)/aug-cc-pVTZ level.[34] However, Grimme's B97-D seems to be a promising approach for routine studies of π-π stacking interactions of large curved carbon networks.[29] Therefore, in order to verify the above results, interaction energies were computed at B97-D and M06-2X with 6-31+G** basis set.

Energy decomposition analysis (EDA) was performed by using the energy decomposition scheme of the Amsterdam density functional (ADF) 2012.01 program[42, 43] at the M06-2X/TZ2P level of theory. We used ADF code for its ease of use and relatively exact treatment of decomposition energy that offers the total binding energy with respect to the defined fragments. In EDA, the total interaction energy E_{int} between the interacting fragments is divided into three parts:[44-46]

$$E_{int} = E_{elstat} + E_{Pauli} + E_{orb} \quad (2)$$

where, E_{elstat} is the electrostatic interaction, E_{Pauli} is termed Pauli repulsion and the final term E_{orb} is orbital interaction.

It is well known that the NLO properties are induced by nonlinear charge displacements that are generated under a strong electric field of light. In the presence of weak and static electric field, the energy of a molecule is a function of the field strength. The energy of the perturbed system is described by the expansion:[47, 48]

$$E = E^0 - \mu_i F_i - (\frac{1}{2!})\alpha_{ij} F_i F_j - (\frac{1}{3!})\beta_{ijk} F_i F_j F_k - (\frac{1}{4!})\gamma_{ijkl} F_i F_j F_k F_l + ... \quad (3)$$

where E^0 is the molecular energy in the absence of the applied electric field; μ_i is the molecular permanent dipole moment along the *i* direction; F_i is the Cartesian component of the applied electric field along the *i* direction; α_{ij}, β_{ijk} and γ_{ijkl} are the polarizability, first, and second hyperpolarizability tensors, respectively; and *i, j,* and *k* designate the different components along the *x*, *y* and *z* directions, respectively. The isotropic average polarizability (α_{ave}) is calculated as:[49]

$$\alpha = \alpha_{ave} = \frac{1}{3}(\alpha_{xx} + \alpha_{yy} + \alpha_{zz}) \quad (4)$$

The orientationally averaged second hyperpolarizability (γ) has been calculated by using the following expression:

$$\gamma = \gamma_{tot} = \frac{1}{5}(\gamma_{xxxx} + \gamma_{yyyy} + \gamma_{zzzz} + 2\gamma_{xxyy} + 2\gamma_{xxzz} + 2\gamma_{yyzz}) \quad (5)$$

When it comes to the calculation of α and γ, three functionals (M06-2X, CAM-B3LYP and ωB97XD) have been chosen. The M06-2X functional was suited to calculate the γ values of such π-stacking dimers.[50] The Coulomb-attenuated hybrid exchange-correlation (CAM-B3LYP) functional is a hybrid functional with improved long-range properties.[51] The ωB97XD functional is the long-range corrected hybrid density functional with damped atom-atom dispersion corrections, which appears most promising for calculations on π-dimer systems.[52] Time-dependent DFT (TD-DFT) has nowadays become general tools to the understanding and predicting the behavior of the electron transition property.[53,54] To obtain more insight on the description of the trend of third-order NLO responses, the vertical electronic transition energies between the ground and excited states were calculated using TD-M06-2X.

The transition density matrix (TDM), orbital overlap integral (S_{ij}) and electronic coupling (V_{ij}) were obtained by Multiwfn software Version 3.3.7.[55] All DFT and TD-DFT calculations in this work were carried out using Gaussian 09W package.[56] The reduced density gradient isosurface was plotted using VMD 1.9.1.74.[57]

3. Results and discussion

3.1 Geometrical structure

The equilibrium structures of the dimers were obtained by M06-2X functional (Fig. 1). The distance between the center of five-member ring in $C_{20}H_{10}$ monomers of **1a** is 3.63 Å (Table 1), which is very close to 3.64 Å that obtained at the QCISD(T)/aug-cc-pVTZ[29] and SCS-MP2/cc-pvtz[31] level of theory by Andrzej Sygula and Svein Saebø suggesting that M06-2X functional is an efficient and reliable functional to study the dimers. The layer distance of **2a** (3.32 Å) is smaller than that of **1a**. Similar results are also founded between **2b** (3.84 Å) and **1b** (3.88 Å). It indicates that the layer distance of convex-convex dimers are smaller as compared to that of concave-convex dimers. However, the concave-convex dimers show much lower energies with respect to the convex-convex dimers, indicating the more stable concave-convex dimers.

Furthermore, we calculated the binding energies (Table 1, E_{int}^{a}) to understand the stability. It is revealed that M06-2X underestimates when compared to the high level ab initio calculations at the counterpoise corrected QCISD/aug-cc-pVTZ level (15.5 kcal/mol). Unsurprisingly, the binding energies in corannulene dimer are best reproduced at B97-D/6-31+G** (15.5 kcal/mol), coinciding exactly with that of the benchmark calculations of 15.5 kcal/mol at QCISD/aug-cc-pVTZ. The computed results showed that E_{int}^{a} (B97-D) values follow the trend: **1a** (15.55 kcal/mol) > **2a** (8.59 kcal/mol) and **1b** (45.27 kcal/mol) > **2b** (36.71 kcal/mol), indicating that the strong binding interactions are beneficial for the stability of the dimerization. Moreover, The interaction energies estimated by B97-D and M06-2X calculations for the eclipsed concave-convex model of corannulene dimer with various basis sets were summarized in Table S1. Results show that the better results of B97-D are correspond to the smaller basis sets.

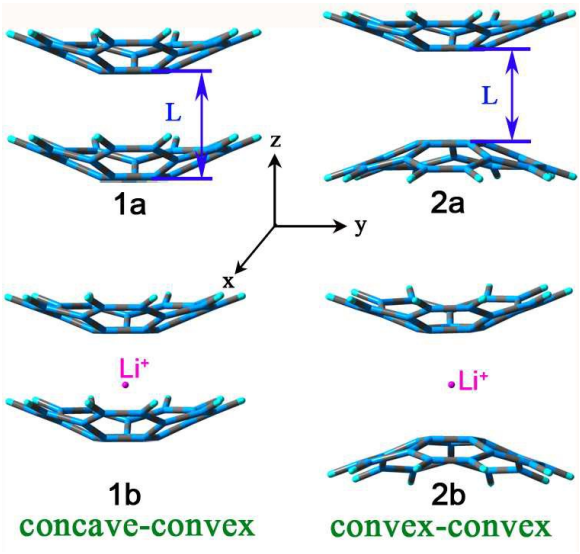

Fig. 1 Eclipsed structures of $C_{20}H_{10}$ and its Li-doped dimers.

Table 1 Layer distances (L, Å), relative energies (E_{rel}, kcal/mol) of the studied dimers and interaction energies (E_{int}[a], kcal/mol) obtained by B97-D and M06-2X functionals.

Dimers	L	E_{rel}	E_{int}[a] (B97-D)	E_{int}[a] (M06-2X)
1a	3.63	0.00	-15.55	-13.75
2a	3.32	11.66	-8.59	-2.64
1b	3.88	0.00	-45.27	-34.94
2b	3.84	10.13	-36.71	-25.30

[a] obtained by Gaussian program

3.2 Nature of the interactions in the dimers

To provide further insight into the nature of the intermolecular interactions in these dimeric species, the EDA was performed to arrive at the relative contributions of various energy terms toward the total intermolecular energy. The absolute interaction energies E_{int}[b] (Table 2) follow the trend: **1a** (13.95 kcal/mol) > **2a** (3.45 kcal/mol) and **1b** (41.62 kcal/mol) > **2b** (23.51 kcal/mol). It is noted that the E_{int}[b] values are quite close to those E_{int}[a] (M06-2X) values from Table 1 and their predicted stability sequences are also fully identical (Fig. 2). The slightly different values between E_{int}[a]

and E_{int}^{b} may be due to the different basis sets. We also note that all of dimers have negative E_{elstst} and E_{orb} values, indicating that the electrostatic and orbital interactions play important role roles in the stability of these cases.

Notice the significant contribution of the dispersion interactions term, E_{elstst}, it reveals that the concave-convex dimers (**1a** and **1b**) possess larger E_{elstst} values when compared to the convex-convex dimers (**2a** and **2b**), which is in line with the E_{int}^{b}. The difference of E_{elstst} between concave-convex and convex-convex dimers is large enough (8.2 kcal/mol and 11.11 kcal/mol, respectively) to distinguish. However, the differences of E_{orb} and E_{pauli} between concave-convex and convex-convex dimers are quite small. Therefore, among all interaction energies, electrostatic interaction, which arises in the molecular crystals of aromatic molecules, plays a pivotal role in determining the energetically accessible stacking motifs. In addition, a linear relationship is founded between E_{orb} and E_{int} (Fig. 2), suggesting that E_{orb} value makes a major contribution to E_{int}^{b}. Additional, Li-doped dimers (**1b** and **2b**) possess relatively larger E_{int}^{b} values because of the enhancement of E_{orb} compared with **1a** and **2a**, suggesting that the doping of Li ion significantly enhances the orbital interaction between the monomers.

Table 2 Results of EDA at the M06-2X/TZ2P level for $C_{20}H_{10}$ monomers as fragments (energies in kcal/mol)).

Dimers	E_{elstst}	E_{pauli}	E_{orb}	E_{int}^{b}
1a	-11.33	5.04	-7.67	-13.95
2a	-3.13	2.93	-3.25	-3.45
1b	-14.08	8.22	-35.76	-41.62
2b	-2.97	13.06	-33.59	-23.51

[b] obtained by ADF program

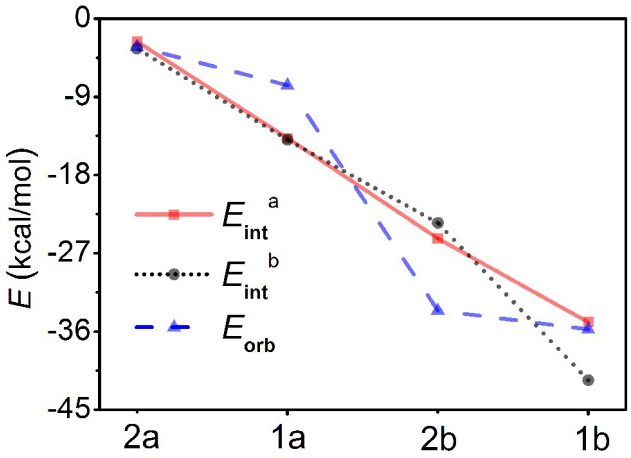

Fig. 2 The corresponding relationships between E_{int}^{a}, E_{int}^{b} and E_{orb}.

To distinguish three different types of noncovalent interactions (i.e., hydrogen-binding, van der Waals interaction and steric hindrance), low-gradient isosurfaces (s = 0.5 a.u.) for the dimers (Fig. 3) were plotted. It is an approach to detect noncovalent interaction in real space, based on the electron density and reduced gradient proposed by Yang *et al*.[58] The surfaces are colored on a red-green-blue scale according to values of sin(λ)ρ, ranging from -0.04 to 0.02 a.u. Blue indicates strong attractive interactions (like hydrogen binding), the transition region (green) indicates typical van der Waals interaction, and red indicates strong steric hindrance.

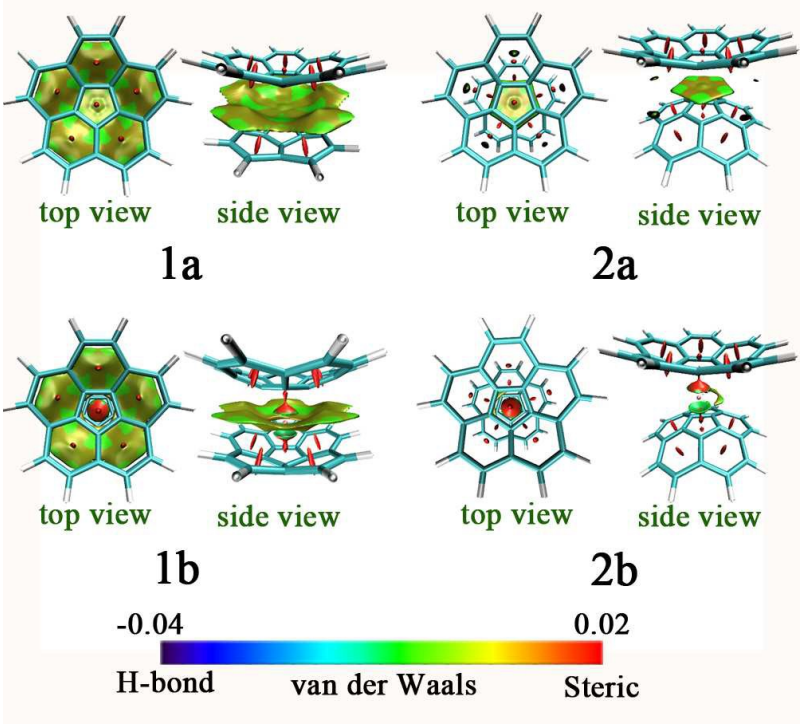

Fig. 3 Gradient isosurfaces (s = 0.5 a.u.) of optimized structures for the dimers.

The interaction region of **1a** marked by large green circle can be identified as van der Waals interaction region because the filled-color is green or light brown, meaning that the density electron in this region is low. In the case of **2a**, small green circle is observed between the central five-member rings of $C_{20}H_{10}$ monomers. In fact, the weak interaction region in **1a** is with more green and light-brown area than those of **2a**. Similar comparative result can be observed in **1b** and **2b**. It can be easily conclude that the π-π interactions between the monomers of the concave-convex dimers (**1a** and **1b**) are stronger with reference to that of the convex-convex dimers (**2a** and **2b**), which is well in agreement with the larger E_{int} in the concave-convex dimers.

3.3 Electronic absorption spectrum

In order to obtain a more intuitive description of the band assignments of the electronic absorption spectra and the trends in the NLO behaviors of the studied dimers, TD-DFT calculations were carried out at the M06-2X functional. The excited-state transition energies (eV), oscillator strengths (*f*), and relevant molecular

orbitals of all complexes in singlet excited-state transitions are summarized in Table S2. To rationalize the observed spectral properties, the differences in the absorption spectra between the dimers are presented (Fig. 4).

Absorption spectrum of **1a** is characterized by two broad absorption (low-energy and high-energy) in the ultraviolet region. Compared with the absorption spectrum of **1a**, additional small peak of the low-energy absorption band appears in the spectrum of **2a** at 299.4 nm. Moreover, the relatively lower energy absorption peak of **2a** at 253.4 nm with higher oscillator strength was 1 nm red-shifted in relation to the corresponding spectrum of **1a**. It indicates that dimer **2a** with smaller transition energies is more vulnerable to occur the electron transition, thus exhibits relatively larger second hyperpolarizability. Coming to Li-doped dimers, the simulated absorption spectrum of **2b** is qualitative quite similar to that of **1b**, *i.e.*, exhibiting one high-energy electronic transition absorbing at 221.6 nm (215.2 nm for **1b**) along with an intense low-energy electronic transition of higher intensity absorbing at 254.1 nm (266.6 nm for **1b**). The low-energy band of **2b** is red-shifted with respect to the corresponding electronic transition in the spectrum of **1b**, suggesting that **2b** may exhibit relatively large second hyperpolarizability. It is must mentioned that **1b** and **2b** show the similar low- and high-energy absorptions as compared with **1a** and **2a** (with exception of different intensity), respectively, indicating the small Li-doped effect on the spectra of the dimers.

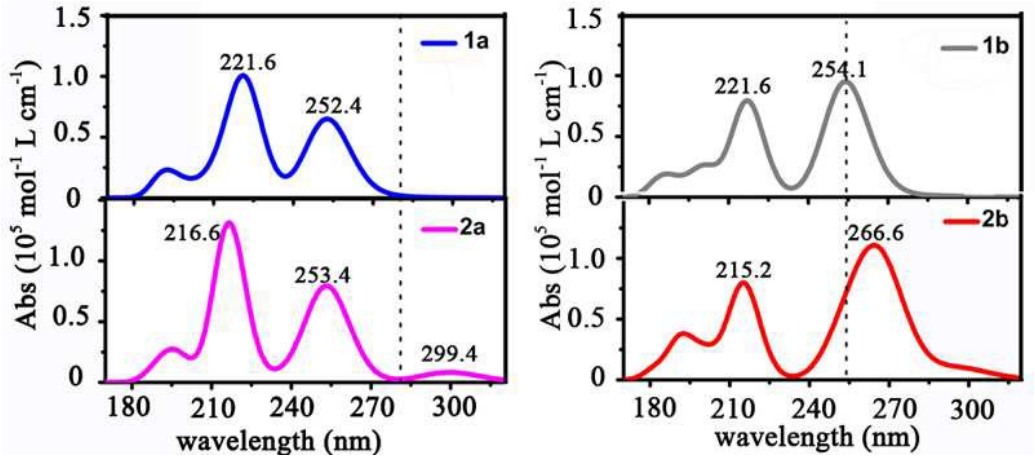

Fig. 4 Absorption spectra of the dimers.

3.4 The static polarizability and second hyperpolarizability

For the studied dimers, the first hyperpolarizability (β) vanishes because of their centrosymmetry, thus, the polarizability (α) and the second hyperpolarizability (γ) will be discussed. Tensor components of γ value were also investigated to understand the fundamental component. Since no experimental or theoretical results of γ values have been currently available for the studied dimers, a comparative discussion of the results (Table 3) obtained by different DFT methods is useful. It can be noted that the α and γ values of M06-2X, ωB97XD and CAM-B3LYP functionals vary within a close margin. To discuss these results in more detail, we use the data of the M06-2X functional to evaluate the trend of the α and γ values.

The α values (Table 3) of **2a** and **2b** were estimated to be 429.3 a.u. and 430.4 a.u., somewhat higher compared to that of **1a** and **1b** (408.4 a.u. and 404.8 a.u.). It suggests that the convex-convex dimers posses larger α values compared with the concave-convex ones. In order to provide an original understanding of the α values, we focused on the relative electronic spatial extent $\langle R^2 \rangle$. The $\langle R^2 \rangle$ values in series decrease as **2b** (1.4×10^4 a.u.) > **2a** (1.2×10^4 a.u.) > **1a** (1.0×10^4 a.u.) ≈ **1b** (1.0×10^4 a.u.), which is in well accordance with the decreasing order of the α values (Fig. 5). To the best of our knowledge, the $\langle R^2 \rangle$ is a physical property that characterizes the electron density volume around the molecule.[59] The more diffuse electron cloud may lead to a larger $\langle R^2 \rangle$ value, resulting in a larger α value.

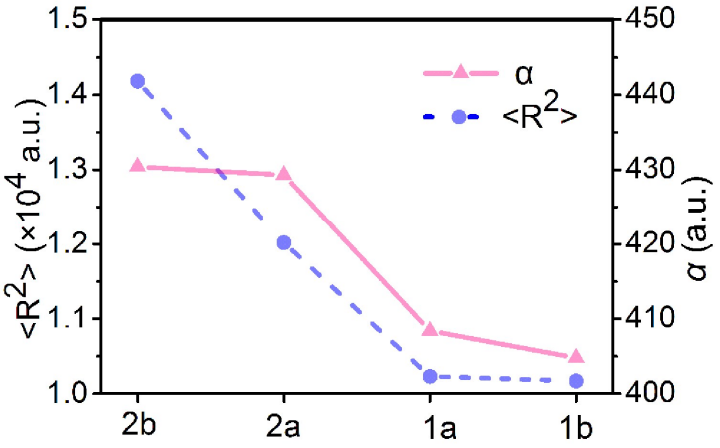

Fig. 5 Relationship between the α values and the corresponding $<R^2>$values for the four dimers.

Moving to the γ values of the dimers, as expected, the convex-convex dimers (**2a** and **2b**) exhibit larger γ values with respect to the concave-convex dimers (**1a** and **1b**) because of smaller transition energies, their γ values follow the trend: **2a** (1.2×10^5 a.u.) > **1a** (1.0×10^5 a.u.) and **2b** (1.1×10^5 a.u.) > **1b** (7.8×10^4 a.u.). The results also reveal that doping Li ion can not significantly influence the γ values. It is consistent with the information obtained when calculating absorption spectra, that is, the small Li-doped effect on the spectra of the dimers. Taking notice of the tensor components for **1a** and **1b**, the γ_{xxxx} and γ_{yyyy} values are the dominating components. Whereas, the highest static γ values of **2a** and **2b** are noticed for the γ_{zzzz} component. It shows that the γ_{zzzz} values for the convex-convex dimers **(2a** and **2b)** are larger (of 95.7 a.u and 138.2 a.u, respectively) with respect to that of concave-convex dimers (**1a** and **1b**). Note also that γ_{zzzz} values follow a similar trend to γ values. It is easy to reach the conclusion that the remarkably large γ values of the convex-convex dimers are due to the strong enhancement of the γ_{zzzz} longitudinal components. The results indicate that the CT trasition along the *z*-axis between two $C_{20}H_{10}$ monomers partly takes place, which can be reasonably explained by the TDM as described below.

Table 3 Total polarizability α (a.u.), second hyperpolarizability γ ($\times 10^3$ a.u.) and electronic spatial extent $<R^2>$ (a.u.) of the dimers computed at various levels of theory.

Dimers	Functionals	$<R^2>$	α	γ	γ_{xxxx}	γ_{yyyy}	γ_{zzzz}
1a	M06-2X	10231	408.4	101.4	117.5	117.6	88.1
	ωB97XD	—	407.4	118.8	121.9	122.0	149.5
	CAM-B3LYP	—	408.3	110.0	127.8	127.8	89.5
2a	M06-2X	12021	429.3	120.4	117.5	117.4	183.8
	ωB97XD	—	428.1	125.4	122.5	122.5	180.5
	CAM-B3LYP	—	429.2	129.1	126.9	126.9	184.8
1b	M06-2X	10170	404.8	77.7	89.2	89.2	69.1
	ωB97XD	—	403.5	73.5	90.4	90.4	44.9
	CAM-B3LYP	—	404.2	79.6	93.9	93.8	65.8
2b	M06-2X	14183	430.4	109.8	96.3	95.8	207.3
	ωB97XD	—	429.1	97.3	98.5	98.1	134.0
	CAM-B3LYP	—	431.0	106.1	101.7	101.3	164.2

The molecular second-hyperpolarizability (γ) which evaluates the third-order NLO efficiency, can be predicted from two-level model[60] that links the γ value and the low-lying CT character γ^{2L}.

$$\gamma^{2L} \propto \frac{f_{gm}^2}{E_{gm}^5} \tag{6}$$

where f_{gm} is the oscillator strength, and E_{gm} is the transition energy. Hence, the E_{gm} and f_{gm} values might be considered as the decisive factors in effecting the γ values. The spectroscopic parameters corresponding to the relatively lower energy and higher oscillator strength electronic transition and low-lying CT character γ^{2L} are listed in Table 4. The γ^{2L} order of the dimers decreases as: **2a** (1.01×10^{-4} a.u.) > **1a** (5.47×10^{-5} a.u.) and **2b** (1.95×10^{-4} a.u.) > **1b** (1.49×10^{-4} a.u.), in quantitative agreement with the order of their γ values. The monotonic dependence of the second hyperpolarizabilities

on the γ^{2L} values indicates that the crucial excited states are very important in the discussion on the second hyperpolarizabilities. And in some extent, the γ^{2L} values reproduce qualitative trends correctly and account for a large part of the second hyperpolarizabilities.

Table 4 Absorption wavelengths (λ_{gm}, nm), excited transition energies (E_{gm}, eV), oscillator strengths (f_{gm}), and low-lying CT character γ^{2L} (10^{-4}) values of the dimers.

Dimers	State	λ_{gm}	E_{gm}	f_{gm}	γ^{2L}	MO transitions
1a	23	252.4	4.91	0.3951	0.5470	H-7→L (29%), H-6→L+1 (29%)
2a	16	253.4	4.89	0.5323	1.0134	H-5→L+1 (38%), H-4→L (38%)
1b	19	254.1	4.88	0.6421	1.4897	H-1→L+2 (24%), H→L+3 (22%), H-5→L+1 (14%), H-4→L (12%)
2b	15	266.6	4.65	0.6503	1.9452	H-5→L (46%), H-4→L+1 (46%)

Following, to further understand the origin of the transition property, we focused on electron-hole coherence investigated by means of the transition density matrix (TDM) and the molecular orbitals of the crucial transition states of the four dimers (Fig. S1-S4). TDM is a helpful tool for analyzing electronic excitation processes and providing additional information on electron-hole coherence of specific excitation.[61] The hydrogen atoms have been omitted since they usually have little contribution to the transitions in the TDM.

Inspection of **1a** (Fig. 6) reveals that the electron-hole pairs of the 23th excited state are mainly localized along the diagonal element and still a very little delocalized along the off-diagonal element. These electronic transitions could be assigned as CT character within the two respective monomers along with less interlayer CT between the two monomers. However, for 16th excited state of **2a,** an increase degree of electron-hole coherence are delocalized along the off-diagonal element, indicating the enhanced interlayer CT between the two monomers. The enhanced interlayer CT in **2a** brings about much stronger polarization of $C_{20}H_{10}$ monomers with respect to **1a**. The

polarization lead to strong enhancement of the γ_{zzzz} value of **2a** compared to **1a**. The same result can be observed in the plot of TDM of dimers **1b** and **2b**. Apparently, the enhanced interlayer CT characters are observed in the convex-convex dimers (**2a** and **2b**), resulting in larger γ_{zzzz} values.

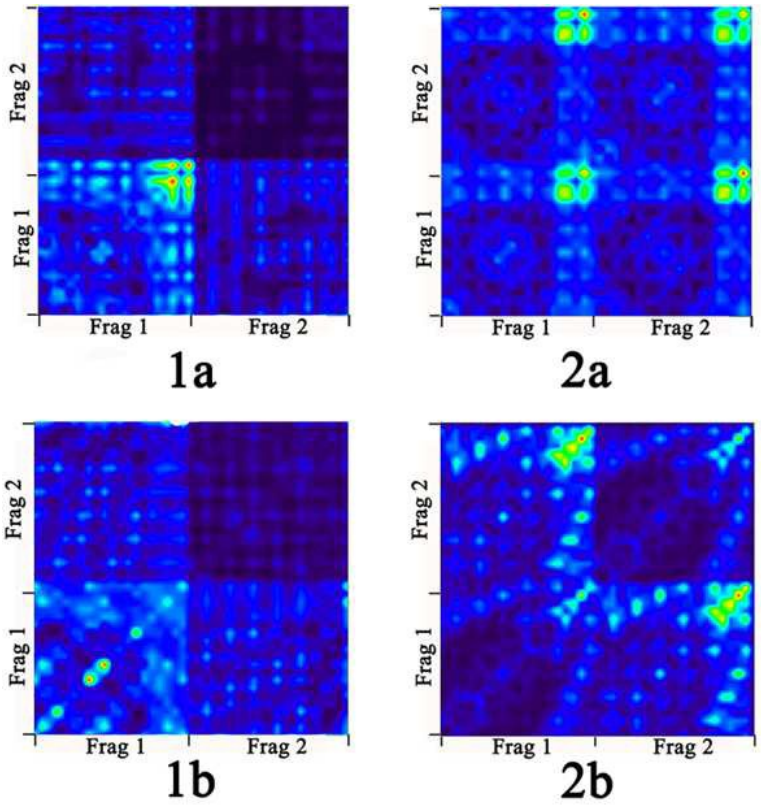

Fig. 6 The TDM corresponding to crucial electronic transitions of dimers **1a** and **2a** (upper layer of the dimer is named as Frag 1, while the lower layer is Frag 2).

In the above dimers, the low-energy peaks can be assigned to the mixture of intralayer CT within the respective monomers and interlayer CT between the two monomers. In fact, the obvious interlayer CT of the convex-convex dimer is partly due to the large overlap between the orbitals of two monomers. The orbital overlap integral (S_{ij}) between two monomers is:[62, 63]

$$S_{i,j}^{Intmol} = \int \varphi_i^{Monomer1}(r)\varphi_j^{Monomer2}(r)dr \quad (7)$$

where i and j are molecular orbital indices of monomer 1 and monomer 2, respectively.

In addition, the electronic coupling between monomers plays a key-role in determining the effective coupling and thus the rate of the single step CT process. The electronic coupling V_{ij} is defined as:[64]

$$V_{ij} = CS_{ij} (C = -0.716 \pm 0.002) \quad (8)$$

This integral is useful in discussions of intermolecular CT.

The absolute V_{ij} order of HOMOs (Table S3) of the dimers decreases as: **2b** (0.975 a.u.) > **2a** (0.080 a.u.) > **1a** (0.009 a.u.) >**1b** (0.003 a.u.). Interestingly, there was an increasing linear relationship between electronic coupling (V_{ij}) and γ_{zzzz} values (Fig. 7). This is due to the fact that the interlayer orbital overlap provides the pathway for the redistribution of electronic charges, thus enhance the interlayer CT characters. Hence, large γ_{zzzz} values relie on the enhancement of electronic coupling (V_{ij}) between HOMOs of two monomers of the convex-convex dimers (**2a** and **2b**).

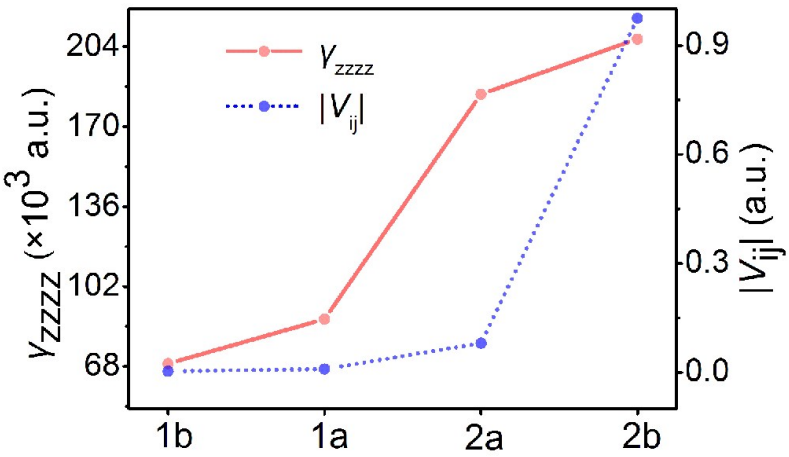

Fig. 7 Relationship between the γ_{zzzz} values and the corresponding $|V_{ij}|$ values for the four dimers.

3.5 The frequency-dependent second hyperpolarizability

The frequency dependent second polarizabilities relevant to the photoelectric Kerr's effect, $\gamma^{EOKE}(-\omega; \omega, 0, -0)$, and the second harmonic generation, $\gamma^{SHG}(-2\omega; \omega, \omega, 0)$, were performed at the M06-2X/6-31+G(d, p) (6-311+G(3df) basis set for the Li ion) level of theory. Generally, γ^{SHG} have been measured in a fundamental incident

wavelength which has a second harmonic far enough from the absorption bands to avoid the over measurement of γ values due to resonance effects. Hence, according to the maximum absorption of **2a** at about 299.4 nm, we investigated the frequency dispersion at wavelength of 1.340 mm (ω= 0.0340 a.u.) and 1.907 mm (ω= 0.0239 a.u.). There is a tiniest increase in the frequency dependent γ values (Table 5). For example, frequency dependent γ^{EOKE} and γ^{SHG} values of **1a** increases by a factor of ~1.03 and ~1.07, respectively, when the frequency of the incident field goes from 0.0239 a.u. to 0.0340 a.u.. Similar results canbe observed for γ^{EOKE} and γ^{SHG} values of all dimers implying slight influence of frequency on the γ^{EOKE} and γ^{SHG} values.

Table 5. The frequency-dependent second hyperpolarizabilities (10^3 a.u.).

Dimers	γ^{EOKE} ($-\omega$; ω, 0, -0)		γ^{SHG} (-2ω; ω, ω, 0)	
	1907 nm	1340 nm	1907 nm	1340 nm
1a	99.5	102.0	104.1	111.9
2a	121.6	125.6	128.9	143.4
1b	75.9	77.8	79.4	84.8
2b	105.5	109.3	112.3	124.5

4. Conclusion

In this work, the binding interactions of the dimers have been systematically investigated using the energy decomposition scheme. It is revealed that the concave-convex dimers exhibit the stronger binding interactions and thus are more stable with respect to the convex-convex dimers. Among all interaction energies, the electrostatic interaction plays a pivotal role in determining the energetically accessible stacking motifs. In addition, the doping of Li ion significantly enhances the orbital interaction between the monomers but slightly effects on the spectra and the second hyperpolarizabilities of the dimers. Importantly, the convex-convex dimers exhibit more obvious interlayer charge transfer, leading to larger second hyperpolarizabilities (γ_{zzzz}) as compared to the concave-convex dimers. It shall provide important evidence

for the convex-convex stacking way in enhancing the NLO properties of the π-dimers. Thereby, the convex-convex stacking dimers may be designed as novel smart NLO materials and a new structure-property correlation can be obtained in optimizing the second hyperpolarizability. Interestingly, owing to that obvious interlayer charge transfer properties result form large overlap and electronic coupling between HOMOs of the monomers, there is an increasing linear relationship between electronic coupling and γ_{zzzz} values. The result, concerning the estimate of the contribution of the electronic coupling and orbital overlap, will be helpful in the qualitative application of such convex-convex stacking models as part of excellent NLO materials.

Acknowledgments

The authors gratefully acknowledge the financial support from the National Natural Science Foundation of China (No. 21173035).

References

1. M. Yamada, K. Ohkubo, M. Shionoya and S. Fukuzumi, *J. Am. Chem. Soc.*, 2014, **136**, 13240-13248.
2. G. Casella and G. Saielli, *New. J. Chem.*, 2011, **35**, 1453-1459.
3. J. Kang, D. Miyajima, Y. Itoh, T. Mori, H. Tanaka, M. Yamauchi, Y. Inoue, S. Harada and T. Aida, *J. Am. Chem. Soc.*, 2014, **136**, 10640-10644.
4. L. Zoppi, L. Martin-Samos and K. K. Baldridge, *J. Am. Chem. Soc.*, 2011, **133**, 14002-14009.
5. Q. Stöckl, D. Bandera, C. S. Kaplan, K. H. Ernst and J. S. Siegel, *J. Am. Chem. Soc.*, 2014, **136**, 606-609.
6. T. Bauert, L. Zoppi, G. Koller, A. Garcia, K. K. Baldridge and K. H. Ernst, *J. Phys. Chem. Lett.*, 2011, **2**, 2805-2809.
7. T. Bauert, L. Zoppi, G. Koller, J. S. Siegel, K. K. Baldridge and K. H. Ernst, *J. Am. Chem. Soc.*, 2013, **135**, 12857-12860.
8. Q. Zhang, K. Kawasumi, Y. Segawa, K. Itami and L. T. Scott, *J. Am. Chem. Soc.*, 2012, **134**, 15664-15667.
9. L. Zoppi, L. M. S. Layla, and K. K. Baldridge, *Acc. Chem. Res.*, 2014, **47**, 3310-3320.
10. W. Xiao, D. Passerone, P. Ruffieux, K. Aït. Mansour, O. Gröning, E. Tosatti, J. S. Siegel and R. Fasel, *J. Am. Chem. Soc.*, 2008, **130**, 4767-4771.
11. R. L. Parc, P. Hermet, S. Rols, D. Maurin, L. Alvarez, A. Ivanov, J. M. Quimby, C. G. Hanley, L. T. Scott and J. L. Bantignies, *J. Phys. Chem. C.*, 2012, **116**, 25089-25096.
12. A. Karton, B. Chan, K. Raghavachari and L. Radom, *J. Phys. Chem. A.*, 2013, **117**, 1834-1842.

13. T. F. Headen, C. A. Howard, N. T. Skipper, M. A. Wilkinson, D. T. Bowron and A. K. Soper, *J. Am. Chem. Soc.*, 2010, **132**, 5735-5742.
14. S. M. Mathew, J. T. Engle, C. J. Ziegler and C. S. Hartley, *J. Am. Chem. Soc.*, 2013, **135**, 6714-6722.
15. E. R. Frey, A. Sygula and N. I. Hammer, *J. Chem. Educ.*, 2014, **91**, 2186–2190.
16. M. C. R. Delgado, E. G. Kim, D. A. d. S. Filho and J. L. Bredas, *J. Am. Chem. Soc.*, 2010, **132**, 3375-3387.
17. S. Sanyal, A. K. Manna and S. K. Pati, *ChemPhysChem.*, 2014, **15**, 885-893.
18. W. Y. Wang, N. N. Ma, C. H. Wang, M. Y. Zhang, S.L. Sun and Y. Q. Qiu, *J. Mol. Graphics Modell.*, 2014, **48**, 28-35.
19. H. L. Xu, Z. R. Li, D. Wu, B. Q. Wang, Y. Li, F. L. Gu and Y. Aoki, *J. Am. Chem. Soc.*, 2007, **129**, 2967-2970.
20. W. Y. Wang, N. N. Ma, S. L. Sun and Y. Q. Qiu, *Organometallics*, 2014, **33**, 3341-3352.
21. C. H. Wang, N. N. Ma, X. X. Sun, S. L. Sun, Y. Q. Qiu and P. J. Liu, *J. Phys. Chem. A.*, 2012, **116**, 10496-10506.
22. M. Y. Zhang, C. H. Wang, W. Y. Wang, N. N. Ma, S. L. Sun and Y. Q. Qiu, *J. Phys. Chem. A.*, 2013, **117**, 12497-12510.
23. W. Y. Wang, N. N. Ma, S. L. Sun and Y. Q. Qiu, *Phys. Chem. Chem. Phys.*, 2014, **16**, 4900-4910.
24. N. Ma, L. Yan, W. Guan, Y. Qiu and Z. Su, *Phys. Chem. Chem. Phys.*, 2012, **14**, 5605-5612.
25. W. E. Barth, R. G. Lawton, *J. Am. Chem. Soc.*, 1966, **88**, 380-381.
26. T. Bauert, K. K. Baldridge, J. S. Siegel, K. H. Ernst, *Chem. Commun.*, 2011, **47**, 7995-7997.
27. H. Becker, G. Javahery, S. Petrie, P. C. Cheng, H. Schwarz, L. T. Scott and D. K. Bohme, *J. Am. Chem. Soc.*, 1993, **115**, 11636-11637.
28. M. L. Christian, G. Stefan, K. Lesya and S. Andrzej, *Phys. Chem. Chem. Phys.*, 2010, **12**, 7091-7097.
29. T. Janowski, P. Pulay, A. A. Sasith Karunarathna, A. Sygula and S. Saebø, *Chem. Phys. Lett.*, 2011, **512**, 155-160.
30. P. A. Denis, *Chem. Phys. Lett.*, 2011, **516**, 82-87.
31. A. Sygula and S. Saebø, *Int. J. Quantum. Chem.*, 2009, **109**, 65-72.
32. D. Josa, J. Rodriguez Otero and E. M. Cabaleiro Lago, *Phys. Chem. Chem. Phys.*, 2011, **13**, 21139-21145.
33 M. R. Kennedy, L. A. Burns and C. D. Sherrill, *J. Phys. Chem. A.*, 2012, **116**, 11920-11926.
34. D. Josa, J. Rodriguez Oteroand, E. M. Cabaleiro Lago and M. Rellan Pineiro, *Chem. Phys. Lett.*, 2013, **557**, 170-175.
35. C. G. Liu, Y. Q. Qiu, Z. M. Su, G. C. Yang and S. L. Sun, *J. Phys. Chem. C.*, 2008, **112**, 7021-7028.
36. N. N. Ma, S. L. Sun, C. G. Liu, X. X. Sun and Y. Q. Qiu, *J. Phys. Chem. A.*, 2011, **115**, 13564-13572.
37. N. N. Ma, S. J. Li, L. K. Yan, Y. Q. Qiu and Z. M. Su, *Dalton Transactions*, 2014, **43**, 5069-5075.
38. L. Wang, W. Y. Wang, N. N. Ma, D. M. Tian, J. Wang and Y. Q. Qiu, *J. Mol. Graphics Modell.*, 2015, **55**, 33-40.
39. Y. Zhao and D. Truhlar, *Theor. Chem. Acc.*, 2008, **120**, 215-241.

40. Y. Zhao and D. G. Truhlar, *Acc. Chem. Res.*, 2008, **41**, 157-167.
41. L. M. da Costa, S. R. Stoyanov, S. Gusarov, X. Tan, M. R. Gray, J. M. Stryker, R. Tykwinski, J. W. de M. Carneiro, P. R. Seidl and A. Kovalenko, *Energy Fuels*, 2012, **26**, 2727-2735.
42. ADF 2012.01 SCM; Theoretical Chemistry, Vrije Universiteit: Amsterdam, http://www.scm.com.
43. C. Fonseca Guerra, J. G. Snijders, G. te Velde and E. J. Baerends, *Theor. Chem. Acc.*, 1998, **99**, 391-403.
44. M. Contreras, E. Osorio, F. Ferraro, G. Puga, K. J. Donald, J. G. Harrison, G. Merino and W. Tiznado, *Chem. Euro. J*, 2013, **19**, 2305-2310.
45. G. Gayatri, Y. Soujanya, I. Fernández, G. Frenking and G. N. Sastry, *J. Phys. Chem. A.*, 2008, **112**, 12919-12924.
46. A. Diefenbach, F. M. Bickelhaupt and G. Frenking, *J. Am. Chem. Soc.*, 2000, **122**, 6449-6458.
47. Y. Q. Qiu,* H. L. Fan, S. L. Sun, C. G. Liu, and Z. M. Su, *J. Phys. Chem. A.*, 2008, **112**, 83-88.
48. W. Y. Wang, X. F. Du, N. N. Ma, S. L. Sun and Y. Q. Qiu, *J. Mol. Model.*, 2013, **19**, 1779 – 1787.
49. J. Tong, Y. Li, D. Wu, Z. R. Li and X. R. Huang, *J. Phys. Chem. A.*, 2010, **114**, 5888-5893.
50. A. Alparone, *Chem. Phys. Lett.*, 2011, **514**, 21-25.
51. A. Pedone, *J. Chem. Theory Comput.*, 2013, **9**, 4087-4096.
52. U. Salzner and A. Aydin, *J. Chem. Theory Comput.*, 2011, **7**, 2568-2583.
53. D. Casanova, F. P. Rotzinger and M. Grätzel, *J. Chem. Theory Comput.*, 2010, **6**, 1219-1227.
54. S. Meng, E. Kaxiras, M. K. Nazeeruddin and M. Grätzel, *J. Phys. Chem. C.*, 2011, **115**, 9276-9282.
55. T. Lu and F. W. Chen, *J. Comput. Chem.*, 2012, **33**, 580–592.
56. M. J. Frisch, G. W. Trucks, H. B. Schlegel, G. E. Scuseria, M. A. Robb, J. R. Cheeseman, G. Scalmani, et al. Gaussian 09, Revision D.01; Gaussian, Inc.: Wallingford, CT, 2009.
57. W. Humphrey, A. Dalke and K. Schulten, VMD: Visual molecular dynamics. *J. Mol. Graphics.,* 1996, **14**, 33-38.
58. E. R. Johnson, S.Keinan, M. S. Paula , C. G. Julia, A. J. Cohen and W. Yang, *J. Am. Chem. Soc.,* 2010, **132**, 6498 – 6506.
59. D. Scuderi, A. Paladini, M. Satta; D. Catone, S. Piccirillo, M. Speranza, A. G. Guidoni, *Phys. Chem. Chem. Phys.*, 2002, **4**, 4999–5003.
60. K. Hatua and P. K. Nandi, *J. Phys. Chem. A.*, 2013, **117**, 12581-12589.
61. W. Y. Wang, Y. H. Kan, L. Wang, S. L. Sun and Y. Q. Qiu, *J. Phys. Chem. C.*, 2014, **118**, 28746-28756.
62. E. W. Castner, D. Kennedy and R. J. Cave, *J. Phys. Chem. A.*, 2000, **104**, 2869-2885.
63. E. W. Schlag, D. Y. Yang, S. Y. Sheu, H. L. Selzle, S. H. Lin and P. M. Rentzepis, *PNAS*, 2000, **97**, 9849-9854.
64. A. Troisi and G. Orlandi, *J. Phys. Chem. B.*, 2002, **106**, 2093-2101.